Electrocatalytic and Solar-Driven Reduction of Aqueous CO_2 with Molecular Cobalt Phthalocyanine-Metal Oxide Hybrid Materials

Souvik Roy[1,2], Melanie Miller[1], Julien Warnan[1,3], Jane J. Leung[1], Constantin D. Sahm[1], Erwin Reisner[1*]

[1] *Department of Chemistry, University of Cambridge, Cambridge CB2 1EW, UK*

[2] *School of Chemistry, Joseph Banks Laboratories, University of Lincoln, Lincoln LN6 7DL, UK*

[3] *Current address: Department Chemie, Technische Universität München, Lichtenbergstraße 4, 85747 Garching, Germany*

Email: reisner@ch.cam.ac.uk

Keywords: CO_2 reduction, artificial photosynthesis, molecular catalysts, hybrid materials, cobalt phthalocyanine, electrochemistry

Abstract

Electrolytic or solar-driven reduction of CO_2 to CO using heterogenized molecular catalysts is a promising approach towards production of a key chemical feedstock, as well as mitigating CO_2 emissions. Here, we report a molecular cobalt-phthalocyanine catalyst bearing four phosphonic acid anchoring groups (**CoPcP**) that can be immobilized on metal oxide electrodes. A hybrid electrode with **CoPcP** on mesoporous TiO_2 (*meso*TiO_2) converts CO_2 to CO in aqueous electrolyte solution at a near-neutral pH (7.3) with high selectivity and a turnover number for CO (TON_{CO}) of 1949 ± 5 after 2 h controlled potential electrolysis at –1.09 V *vs.* SHE (~550 mV overpotential). In situ UV-visible spectroelectrochemical investigations alluded to a catalytic mechanism that involves non-rate-limiting CO_2 binding to the doubly-reduced catalyst. Finally, the integration of the *meso*TiO_2|**CoPcP** assembly with a *p*-type silicon (Si) photoelectrode allowed the construction of a benchmark precious-metal-free molecular photocathode that achieves a TON_{CO} of 939 ± 132 with 66% selectivity for CO ($CO/H_2 = 2$) under fully aqueous condition. The electrocatalytic and photoelectrochemical (PEC) activity of **CoPcP** was compared to state-of-the-art synthetic and enzymatic CO_2 reduction catalysts, demonstrating the excellent performance of **CoPcP** and its suitability for the integration in tandem PEC devices.

Introduction

The renewable conversion of CO_2 and water to storable fuels and chemicals offers a promising route to a sustainable economy employing a closed carbon cycle. The reduction of CO_2 can be powered by renewable electrical and solar energy in electrolysis and photoelectrochemical (PEC) devices, respectively.[1] However, the direct electroreduction of aqueous CO_2 on heterogeneous electrodes suffers often from high overpotentials and low product selectivity, and PEC conversion from low photochemical quantum yield and limited solar-to-chemical conversion yields.[2] These drawbacks have inspired the development of molecularly-engineered hybrid materials that can benefit from a CO_2-reducing molecular catalyst with performance advantages such as high selectivity, low overpotential, and tunability as well as high activity per catalytic center.[3-9]

Hybrid photocathodes with molecular catalysts anchored on *p*-type semiconductors (SCs) and positioned at the electrode/electrolyte interface, allow the coupling to water oxidizing anodes without the need for sacrificial reagents and pave the way for unassisted operation during solar irradiation. While a number of such hybrid molecular photocathodes have already been developed for the reduction CO_2, those operating under fully aqueous condition rely on either noble-metal-based catalysts[10-15] or large overpotentials,[16,17] and others require organic solvents with catalysts in solution.[18,19] Photocathodes with a buried *p*-*n* junction feature a small-bandgap *p*-type SC protected by a large-bandgap *n*-type SC layer.[20-25] The narrow-bandgap SC allows broad-band harvesting of solar light, and the protective overlayer prevents photocorrosion and provide a scaffold for attaching molecular co-catalysts. Early reports demonstrated CO production in organic solvents by TiO_2-protected Cu_2O photocathodes with a Re-catalyst under strongly reducing conditions (–1.9 V *vs.* $Fc^{+/0}$).[20,21] A TiO_2-coated hematite photocathode that operates in water to produce CO and formate with $FE_{CO+HCOO^-}$>90% was reported based on polymeric Ru complex catalysts. More recently, we reported a noble-metal-free photocathode consisting of a narrow-bandgap (1.1 eV) *p*-type Si photoelectrode coated with mesoporous TiO_2 (*meso*TiO_2) overlayer to protect Si from reacting with H_2O and O_2 to form of an insulating silica (SiO_x) layer, and provide a high surface area to immobilize a phosphonated Co(bisterpyridine) catalyst.[25] The hybrid system operates with a low overpotential and good selectivity in organic/water mixtures, but performed poorly in purely aqueous electrolyte solution with a low Faradaic efficiency (FE) for CO_2-products and a low turnover number (TON_{CO_2}) of 21.[25] Very recently, a hybrid photocathode featuring a cobalt quaterpyridine catalyst immobilized on *p*-type Cu(In,Ga)Se_2 (CIGS) SC that generates CO with 97% selectivity and high current density in aqueous medium has been reproted.[24] As the molecular catalyst is a key component in the photocathodes generating C1 products at low overpotential, seeking other suitable catalysts/semiconductor assemblies to drive CO_2 reduction catalysts is therefore desirable.

Cobalt phthalocyanine (**CoPc**) has been studied for electrocatalytic CO_2 reduction since the 1970s[26-28] and has attracted renewed attention over the past 5 years due to their excellent performance in water upon immobilization on carbon electrodes,[29-34] and reticular materials.[33,35] A state-of-the-art **CoPc**-based catalyst system features a positively charged **CoPc** complex adsorbed on multiwalled carbon nanotubes, which displays >90% CO-selectivity with a partial current density of 18.1 mA cm^{-2} at a ~550 mV overpotential.[29] However, carbonaceous supports offer low optical transparency, limiting the application of these hybrid **CoPc**-electrodes in PEC systems and rendering spectroscopic studies for mechanistic investigations challenging. We have recently developed a polymeric-**CoPc**/carbon-nitride hybrid photocatalyst for light driven CO_2 reduction in colloidal suspension,[36] but this system relied on a sacrificial electron donor and utilization of **CoPc** in PEC CO_2 reduction has not yet been reported.

Metal oxides (MO_x) present a suitable electroactive platform for catalyst immobilization and PEC application as MO_x materials offer transparency, tunable electronic properties and morphology, and affinity towards various functional groups including phosphonic acid, carboxylic acid and silatrane, that can be exploited for catalyst anchoring.[37-43] However, there are relatively few reports of noble-metal-free molecular CO_2 reduction catalysts that are amenable towards immobilization on MO_x surfaces and all of those feature phosphonic acid anchors: an Fe-porphyrin dimer,[41] a Co-terpyridine,[25] a Mn-bipyridine tricarbonyl,[40] and the recently reported Co-quaterpyridine.[24]

Here, we aim to integrate **CoPc** catalyst into MO_x scaffold to fabricate hybrid materials for PEC CO_2 reduction in water. We prepared a novel cobalt phthalocyanine (**CoPcP**) catalyst bearing four flexible phosphonic acid anchors appended to the phthalocyanine macrocycle (Figure 1A), which allow immobilization of the catalyst on mesoporous MO_x electrodes including indium tin oxide (*meso*ITO) and titanium dioxide (*meso*TiO_2). The resulting hybrid electrode assemblies (*meso*ITO|**CoPcP** and *meso*TiO_2|**CoPcP**) displayed a high loading of **CoPcP** and were studied electrochemically to demonstrate catalytic CO_2 reduction in water and spectroelectrochemically to elucidate mechanistic details. The *meso*TiO_2|**CoPcP** assembly was then integrated on top of a Si photoelectrode to perform solar-driven CO evolution from CO_2 under fully aqueous conditions.

Results and Discussion

The phosphonated CO_2 reduction catalyst **CoPcP** was synthesized in seven steps from the commercially available starting material 4-nitrophthalonitrile in an overall yield of ~2% (Supporting Information, Scheme S1). Zinc-templated cyclization of *p*-methoxybenzyl (PMB)-substituted phthalonitrile (**1**) yielded the symmetric tetra-substituted Zn-phthalocyanine (**2**) with protected hydroxyl groups. Subsequent removal of the PMB group and demetallation produced tetra-hydroxylated free-base phthalocyanine (**4**), which was reacted with (3-bromopropyl)phosphonate to introduce the phosphonate surface anchoring moieties. Metalation of the resulting free-base phthalocyanine (**5**) and subsequent hydrolysis of the phosphonate esters yielded the target complex **CoPcP**, which was isolated and used as a mixture of regioisomers with identical electronic and steric properties.[44] The compounds were characterized by ^1H and ^{13}C nuclear magnetic resonance (NMR) spectroscopy, mass spectrometry, infrared and electronic absorption spectroscopy and elemental analysis (Supporting Information, Experimental Details and Figure S1-S8).

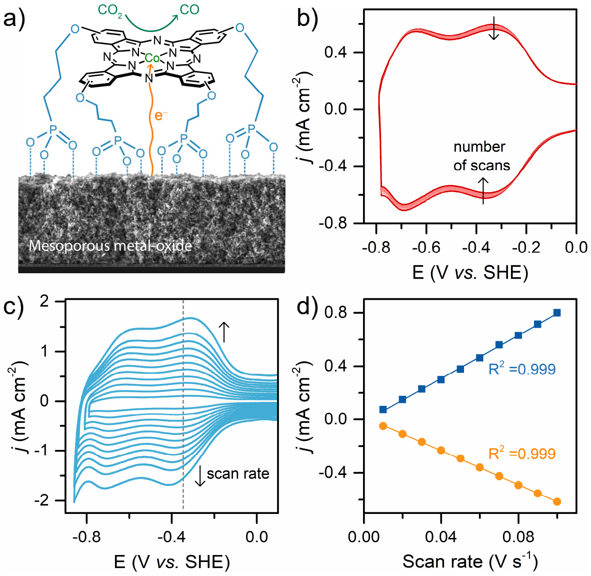

Figure 1. (a) Schematic illustration of CO_2 reduction by **CoPcP** immobilized on mesoporous metal oxide (*meso*ITO and *meso*TiO_2) electrodes. The SEM image on the bottom shows a 5.5 µm thick film of mesoporous indium tin oxide (*meso*ITO). It should be noted that other binding modes of **CoPcP** involving one, two or three phosphonate anchors are also possible. The molecular structure of **CoPcP** is not drawn to scale. (b) Multi-scan CVs of *meso*ITO|**CoPcP** supported on FTO under N_2 at 50 mV s^{-1} showing the scan number 2, 10, 20, 30, 40, 50, 60, 70, 80, 90, and 100 (0.5 M $KHCO_3$, pH 8.6). (c) CVs of FTO|*meso*ITO|**CoPcP** at different scan rates under N_2 (10 to 120 mV s^{-1}, 0.5 M KCl, pH 7.2; KCl was used as the electrolyte to avoid any contribution from HCO_3^- reduction). (d) Correlation with linear fit between the peak current density of the [**CoPcP**]/[**CoPcP**]$^-$ redox process (marked by the dashed line in (c)) and the scan rate. All experiments were performed at room temperature.

CoPcP was immobilized on FTO|*meso*ITO (fluorine doped tin oxide (FTO)-supported *meso*ITO, 5.5 µm film thickness, ITO particle size < 50 nm, geometric surface area 0.36 cm^2; Figure S9) by soaking the electrode in a sensitizing solution of the catalyst (0.2 mM in 2:3 DMSO/MeOH) followed by washing and drying in air. All potentials are reported against standard hydrogen electrode (SHE). As shown in Figure 1b, cyclic voltammograms (CVs) of the FTO|*meso*ITO|**CoPcP** electrode in aqueous electrolyte (pH 8.6, room temperature) showed two well-defined reversible redox processes at $E_{1/2}$ = –0.34 and –0.67 V *vs.* SHE, attributable to a metal-centered [**Co^{II}PcP**]/[**Co^{I}PcP**]$^-$ reduction and a ligand-centered [**Co^{I}PcP**]$^-$/[**Co^{I}PcP$^{•}$**]$^{2-}$ reduction, respectively.[45] Linear dependence of the peak current of the [**Co^{II}PcP**]/[**Co^{I}PcP**]$^-$ process on the scan rate is indicative of an immobilized species in good electronic communication with the electrode (Figure 1c and 1d). The small peak-to-peak separation (~30 mV) at slow scan rates (20 mV s^{-1}) can be assigned to film resistance and further supports a surface-confined electrochemical process. The stable peak currents observed over 100 cycles in multi-scan CVs (Figure 1b) confirmed a robust binding afforded by four phosphonate anchors under non-turnover condition. The coverage of electroactive **CoPcP** ($^{EC}\Gamma_{\mathbf{CoPcP}}$) on the electrode was determined by chronoamperometry as 27 ± 1 nmol cm^{-2} (Figure S10). Desorption of **CoPcP** in basic solution and quantification of the dissolved **CoPcP** by UV-vis spectrophotometry gave an estimate for the total catalyst loading ($^{UV\text{-}vis}\Gamma_{\mathbf{CoPcP}}$) of 24 ± 2 nmol cm^{-2}. The two $\Gamma_{\mathbf{CoPcP}}$ values are in the expected range for metal complexes on nanostructured ITO surfaces,[46,47] and within error of one another, which indicates that all immobilized catalysts were electrochemically accessible (Table S1).

CoPcP was anchored by the same immobilization protocol on Ti foil-supported *meso*TiO_2 electrodes[48] (Ti|*meso*TiO_2; 6.5 µm film thickness, TiO_2 anatase particle size 15–20 nm, geometric surface area = 0.36 cm^2, exposed surface area after epoxy encapsulation = 0.15–0.3 cm^2) to evaluate their CO_2 reduction activity by controlled potential electrolysis (CPE). Ti|*meso*TiO_2 electrodes were selected over FTO|*meso*ITO as they display greater stability while maintaining conductivity at strongly reducing potentials.[49] Immobilization of **CoPcP** was confirmed by X-ray photoelectron spectroscopy (XPS), which showed the expected signals in the Co_{2p}, P_{2p} and N_{1s} regions (Figure 2a and S11). The transmission UV-vis spectrum of *meso*TiO_2|**CoPcP** (supported on FTO-coated glass instead of Ti to enable transparency) showed the characteristic Q-band band at ~678 nm and an additional blue-shifted peak with comparable intensity at ~626 nm (Figure S12a). The presence of the higher energy band is indicative of a face-to-face Co-phthalocyanine aggregate,[50] which suggests that other binding modes of **CoPcP** via one or two phosphonate anchors are also possible (Scheme S3). The $^{UV\text{-}vis}\Gamma_{\mathbf{CoPcP}}$ of the Ti|*meso*TiO_2|**CoPcP** assembly was 23 ± 4 nmol cm^{-2}, which was also corroborated by inductively coupled plasma optical emission spectrometry (ICP-OES) ($^{ICP}\Gamma_{\mathbf{CoPcP}}$ = 25 ± 2 nmol cm^{-2}). Cross-sectional scanning electron microscopy (SEM) and the corresponding energy-dispersive X-ray (EDX) mapping of the *meso*TiO_2|**CoPcP** layer (also deposited on FTO instead of Ti to obtain a clean cross-section) confirms uniform distribution of Co and P throughout the film (Figure S13).

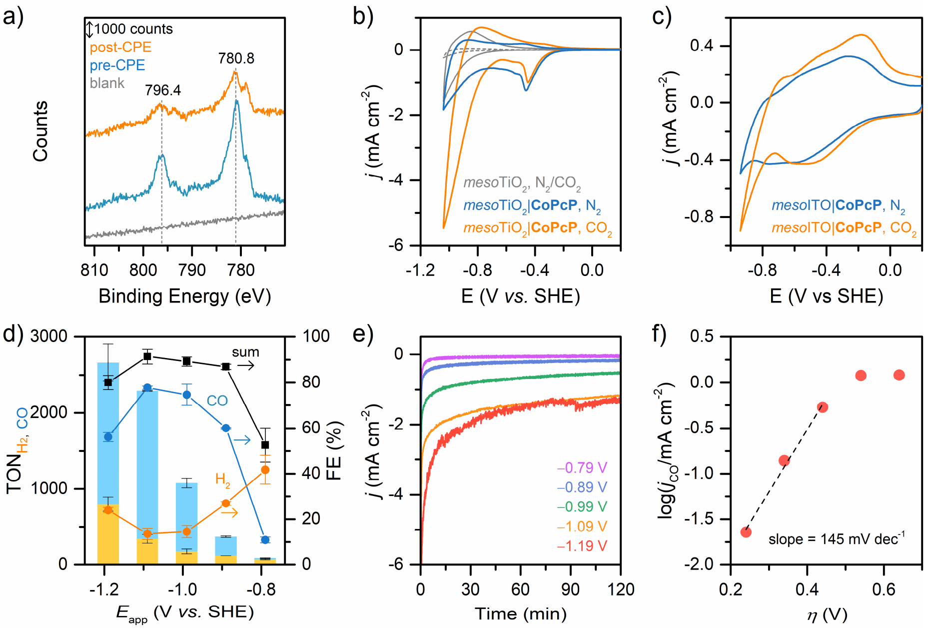

Figure 2. (a) XPS core-level spectra of Ti|*meso*TiO_2|**CoPcP** showing Co_{2p} region before (blue) and after (orange) 2h CPE at –1.09 V *vs.* SHE. Grey trace shows the XPS spectrum of the unmodified Ti|*meso*TiO_2 electrode. (b, c) CVs of Ti|*meso*TiO_2|**CoPcP** (b) and FTO|*meso*ITO|**CoPcP** (c) under N_2 and CO_2 saturation condition; grey traces in (b) show the control experiments with Ti|*meso*TiO_2 under N_2 (dashed line) and CO_2 (solid line). CVs were recorded at 20 mV s^{-1}; 0.5 M KCl and 0.5 M $KHCO_3$ were used as electrolytes for measurements under N_2 and CO_2, respectively. (d, e) Electrocatalytic CO_2 reduction by Ti|*meso*TiO_2|**CoPcP** at different E_{app}: (d) turnover numbers (TON, bar plot) and Faradaic efficiencies (FE, line plot) for evolution of CO (blue) and H_2 (yellow); (e) current density *vs.* time plots. All CPE measurements were conducted in CO_2-saturated 0.5 M $KHCO_3$ (pH 7.3, room temperature). The pH remained unchanged after the CPE. (f) Tafel plot for Ti|*meso*TiO_2|**CoPcP** showing log $|j_{CO}|$ *vs.* η plot derived from the CPE data; $|j_{CO}| = |j| \times FE_{CO}$, where $|j|$ is the current density after 1 h.

The CVs and linear sweep voltammograms (LSVs) of Ti|*meso*TiO_2|**CoPcP** in aqueous KCl solution (pH 7.2) under N_2 displayed the [**CoPcP**]→[**CoPcP**]$^-$ reduction at approximately –0.45 V *vs.* SHE and a second wave with an onset at approximately –0.75 V *vs.* SHE (Figure 2b and S14). Upon CO_2 saturation, an enhanced second wave was observed. A similar current increase was also observed with a *meso*ITO|**CoPcP** electrode (Figure 2c), supporting electrocatalysis. A blank Ti|*meso*TiO_2 electrode exhibited a much lower current under N_2 and CO_2 which corresponds to the filling and emptying of the conduction band of TiO_2 (Figure 2b). Notably, the ratio of cathodic to anodic charge in the forward and reverse CV scans under CO_2 decreased from ~3.9 to ~1.2 upon changing the electrode from Ti|*meso*TiO_2|**CoPcP** to bare Ti|*meso*TiO_2. This suggests that, on the timescale of CV, the conduction band electrons of TiO_2 are consumed by **CoPcP** for catalysis and are therefore unavailable for discharging during the reverse scan. CO_2 reduction by Ti|*meso*TiO_2|**CoPcP** was confirmed by controlled potential electrolysis (CPE) for 2 h in CO_2-saturated $KHCO_3$ (0.5 M, pH 7.3) at selected potentials ranging from –0.79 V to –1.19 V *vs.* SHE (Figure 2d-e). During CPE, the electrochemical cell was constantly purged with CO_2 and the gaseous products were quantified by online gas chromatography (GC) measurements. After CPE, the electrolyte solution was analyzed by ion chromatography for formate and by ^1H NMR spectroscopy for other liquid products. A tabulated summary of CPE results is provided in the Supporting Information, Table S2. Formation of CO was detected at an applied potential (E_{app}) as positive as –0.79 V *vs.* SHE (j_{CO} ~10 μA cm^{-2}), corresponding to an overpotential (η) of 250 mV ($E^{0'}_{CO_2/CO}$ = –0.54 V *vs.* SHE at pH 7.3).[51] However, the selectivity for CO (defined as, $\frac{n_{CO}}{n_{CO} + n_{H_2}} \times 100\%$) at this E_{app} was only (20.7±0.5)%. The current density increased with more reducing potentials and the catalyst displayed a higher selectivity towards CO (Figure 2d-e and S15). A maximum CO selectivity of (85 ± 2)% (CO:H_2 = 5.8 ± 1.0) was reached at E_{app} = –1.09 V *vs.* SHE (j_{CO} ~ –1.3 mA cm^{-2}). CPE for 2 h at this potential generated 44.8 ± 0.1 μmol CO cm^{-2} and 7.8 ± 1.3 μmol H_2 cm^{-2} with a total Faradaic efficiency (FE_{CO+H_2}) of (91±3)%, corresponding to a turnover number of 1949 ± 5 for CO (TON_{CO}) and 340 ± 58 for H_2 (TON_{H_2}). Further lowering E_{app} to –1.19 V promotes H_2 evolution (FE_{CO} = 56 ± 2 and FE_{H_2} = 24 ± 2) leading to a lower CO selectivity of (70 ± 1)% (CO:H_2 = 2.4 ± 0.1). Representative gas chromatogram traces are shown in Figure S16a. No formate was detected in the electrolyte after CPE. It should be noted that the TONs are conservative estimates as they were calculated based on the total **CoPcP** loading on TiO_2. Unlike ITO, the loading of electroactive **CoPcP** on TiO_2 could not be accurately determined from CV experiments due to its semiconducting properties.

The molecular integrity of **CoPcP** was confirmed by XPS and UV-vis spectroscopy analyses of Ti|*meso*TiO_2|**CoPcP** electrodes after 2 h CPE. The XPS spectra show signals at pre-CPE binding energies in the Co_{2p} and P_{2p} regions for Co^{II} and phosphonic acid, respectively (Figure 2a and S11), whereas the optical spectra of the desorbed **CoPcP** display an unchanged Q-band at 678 nm (Figure S12b). The $^{UV\text{-}vis}\Gamma_{\mathbf{CoPcP}}$ was reduced by 20-25% to 18.6 and 17 nmol cm^{-2} after 2 h CPE at –0.99 and –1.09 V *vs.* SHE, respectively (Table S3), suggesting slow catalyst desorption under operating condition due to hydrolysis of the phosphonate ester linkage (**CoPcP** is partially soluble in $KHCO_3$ electrolyte solution). Isotopic labelling experiments conducted in a $^{13}CO_2$-saturated $NaH^{13}CO_3$ solution confirmed formation of ^{13}CO (Figure S16b). Unmodified Ti|*meso*TiO_2 electrode produced only a small amount of H_2 under identical condition (1.28 µmol H_2 after 2 h CPE at −1.09 V *vs.* SHE; Figure S17).

The catalytic activity of **CoPcP** was subsequently compared with two other well-established 3d metal-based molecular catalysts, **MnP** [MnBr(4,4’-bis(phosphonic acid)-2,2’-bipyridine)$(CO)_3$][40] and **CoPolyPc** (polymeric Co-phthalocyanine)[32] (Scheme S2), and a biocatalyst, isolated W-formate dehydrogenase from *Desulfovibrio vulgaris* Hildenborough (**FDH**),[52,53] using *meso*TiO_2 support under fully aqueous condition. FDH was selected as a model enzyme to demonstrate the inherent advantages of the natural system, such as high selectivity and energy efficiency, and to highlight its drawbacks including limited stability and scalability as well as a large catalyst footprint. The procedure for immobilizing **MnP, CoPolyPc** and **FDH** is described in the Supporting Information.

CPE of Ti|*meso*TiO_2|**MnP** at –0.99 and –1.09 V *vs.* SHE produced CO with FE_{CO} of 62% and 39%, corresponding to TON_{CO} of 404 and 276, respectively ($^{ICP}\Gamma_{\mathbf{MnP}}$ = 49.6 nmol cm^{-2}; Figure S18 and Table S2). Unexpectedly, Ti|*meso*TiO_2|**CoPolyPc** primarily catalyzed H_2 evolution with a low CO-selectivity of <5% (Figure S19), even though **CoPolyPc** has been demonstrated to be an excellent CO_2 reduction electrocatalyst when deposited on carbon-nanotubes and possesses an identical Co-phthalocyanine core to that of **CoPcP**. The stark contrast in CO_2 reduction activity between **CoPcP** and **CoPolyPc** could be the flexible phosphonate anchors of **CoPcP**, which provide a distinct molecule-electrode interface.[36] In comparison, the enzyme assembly, *meso*TiO_2|**FDH**, has been previously reported to display an excellent selectivity towards electrochemical reduction of CO_2 to formate with a high TON of ~17,000 and a FE of (92±5)% after 2 h CPE at –0.6 V *vs.* SHE.[54] While the enzyme offered high selectivity with little overpotential requirement,[54] the current density delivered by *meso*TiO2|**FDH** was only ~90 µA cm^{-2} which is considerably lower than that for **CoPcP** and **MnP**. Nevertheless, it should be noted that a much smaller amount of FDH (43 pmol) was employed due to the large footprint of the enzyme and the CPE was conducted at a less negative potential (E_{app} = –0.6 V *vs.* SHE). Overall, the performance for **CoPcP** ($\mathrm{TON_{CO}}$ = 1949 and $\mathrm{FE_{CO}}$ = 78% after 2 h) compares favorably to the two molecular catalysts described here, **MnP** and **CoPolyPc**, and other previously reported molecular catalyst-metal oxide hybrids, including a Fe-porphyrin-based metal-organic framework ($\mathrm{TON_{CO}}$ = 1400 and $\mathrm{FE_{CO}}$ = 40% after 7 h),[55] a Fe-porphyrin dimer deposited on FTO/SnO2 ($\mathrm{TOF_{CO}}$ = 20 s^{-1} and $\mathrm{FE_{CO}}$ = 70%)[41] and a Co-quaterpyridine complex anchored on TiO2 ($\mathrm{TON_{CO}}$ = 1000 and $\mathrm{FE_{CO}}$ = 63% after 2 h). The Ti|*meso*TiO2|**CoPcP** assembly turns over at a slower rate ($\mathrm{TOF_{CO}}$ = 0.27 s^{-1} at –1.09 V *vs.* SHE) compared to other CoPc systems supported on carbon-based electrodes (Table S4), which could be due to slow electron transport across the metal-oxide/**CoPcP** interface as indicated by the peak-to-peak splitting in the CVs at slow scan rate.

To gain kinetic information about CO2 reduction on Ti|*meso*TiO2|**CoPcP**, Tafel analysis was performed by plotting the partial current density for CO (j_{CO}) during CPE on a logarithmic scale (log $|j_{\mathrm{CO}}|$) versus the thermodynamic overpotential (η). A Tafel slope of 145 mV dec^{-1} was obtained in the low-overpotential region (Figure 2f). Although this value is close to the theoretical value of 118 mV dec^{-1} expected for a rate-limiting initial single electron transfer step,[56] there are other key factors, including CO2 adsorption, CO desorption and mass-transport limitation in porous scaffold, that likely exert substantial influence on the Tafel slope of the reaction. For comparison, earlier studies on immobilized phthalocyanine have reported Tafel slopes ranging from 100–300 mV dec^{-1},[57-60] suggesting that it may depend on more than just the active site itself. As a result, mechanistic interpretation and the exact nature of the rate-limiting step is difficult to determine from the Tafel slope alone.

In situ UV-vis spectroelectrochemistry (SEC) under N2 and CO2 was used to study the potential-dependent features of **CoPcP** at a molecular level. A typical spectrum of as-synthesized **Co$^{\mathrm{II}}$PcP** immobilized on ITO and TiO2 in open-circuit states featured two absorptions at 678 and 626 nm in the Q-band range, attributed to the monomer and the aggregate, respectively (Figure 3 and S20).[61] The *meso*ITO|**CoPcP** electrode displays well-separated reduction waves and electrochromic behavior with a change of color from blue to green and dark yellow during CVs (Supporting video S1). The UV-vis spectrum was recorded at –0.47 and –0.71 V *vs.* SHE ascribed to [**Co^{I}PcP**]$^{–}$ and [**Co^{I}PcP$^{\bullet}$**]$^{2–}$, respectively (Figure S20). The reduction of [**Co^{II}PcP**] to [**Co^{I}PcP**]$^{–}$ at −0.47 V *vs.* SHE generated a new Q-band at 658 nm and a broad peak at ~460 nm with isosbestic points at 555 and 717 nm. Lowering the potential to –0.71 V *vs.* SHE led to a red-shift of the Q-band to 717 nm, increase of the charge transfer band at ~440 nm, and isosbestic points at 571 and 708 nm. This is consistent with formation of a Co^{I} center and a reduced phthalocyanine ring (PcP$^{3–}$).[62,63] All spectral changes were fully reversible, indicating that the complex does not undergo any irreversible structural change over the potential window on the time scale of the voltammetric experiment. However, *meso*ITO|**CoPcP** could not be studied under further reducing condition due to limited stability of ITO.

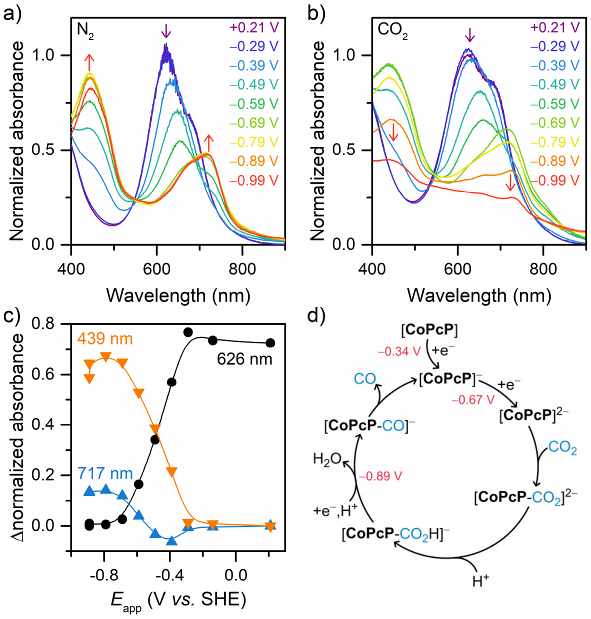

Figure 3. (a-c) In situ UV-vis spectroelectrochemistry of FTO|*meso*TiO$_2$|**CoPcP** conducted under (a) N$_2$ saturated KCl solution and (b) CO$_2$ saturated KHCO$_3$ solution by varying the applied potential from +0.21 to –0.99 V *vs.* SHE. The electrode was held at each potential step for 44 s. Spectra were normalized using the 626 nm band. (c) Potential-dependent changes in the normalized absorbance with a loss of the 626 nm band of **CoPcP** and increase of 439 and 717 nm peaks of [**CoPcP**]$^{2–}$ under N$_2$. (d) Proposed mechanism for CO$_2$ electroreduction by **CoPcP**. Protons are supplied by water or bicarbonate. Two different electrodes were used

for SEC under N_2 and CO_2; slight difference in shape of the initial spectra is caused by varying degree of aggregation in the two electrodes.

A mesoporous TiO_2 scaffold was employed for probing the SEC response of **CoPcP** under operating condition due to its greater stability at strongly reductive potentials. Potential-dependent evolution of the UV-vis spectrum of FTO|*meso*TiO_2|**CoPcP** was nearly identical to that observed for *meso*ITO electrode; **CoPcP** was fully reduced to $[\textbf{CoPcP}]^{2-}$ at –0.69 V *vs.* SHE under both N_2 and CO_2 saturation (Figure 3a, b; and S21), therefore excluding the binding of CO_2 to $[\textbf{CoPcP}]^{-}$. However, the two redox waves are poorly defined in the CVs recorded with *meso*TiO_2|**CoPcP**, leading to overlapping peaks. Plotting the change in absorbance of the bands for **CoPcP** (626 nm) and $[\textbf{CoPcP}]^{2-}$ (439 and 717 nm on *meso*TiO_2) illustrates the coexistence of $[\textbf{CoPcP}]^{-}$ and $[\textbf{CoPcP}]^{2-}$ over a wide potential range, $-0.39\ \text{V} > E_{\text{app}} > -0.69\ \text{V}$ *vs.* SHE (Figure 3c). A partial dip in the 717 nm trace at –0.39 V is caused by the bleach of the 678 band (**CoPcP** monomer), induced by **CoPcP**/$[\textbf{CoPcP}]^{-}$ reduction. Under N_2, the spectrum remained unchanged at more negative potential ($E_{\text{app}} < -0.69$ V *vs.* SHE) suggesting build-up of $[\textbf{CoPcP}]^{2-}$ and no further reaction. In contrast, $[\textbf{CoPcP}]^{2-}$ is consumed under CO_2 saturated condition as $E_{\text{app}} < -0.79$ V *vs.* SHE, as demonstrated by the bleach of the bands at 439 and 717 nm (Figure 3b). This establishes that $[\textbf{CoPcP}]^{2-}$ is not the steady state species during catalysis and a third reduction step occurs at strongly reducing potentials only in the presence of CO_2. The SEC results fits well with the CPE data, which show that H_2 remains the major product until $E_{\text{app}} = -0.79$ V and CO_2 reduction becomes dominant at more negative potentials.

The exact mechanism for CO_2 reduction by cobalt phthalocyanine (**CoPc**) remains a subject of debate in the community.[30,58,64,65] Considering that **CoPcP** displays an onset for CO_2 reduction at a more negative potential than the second reduction and that $[\textbf{CoPcP}]^{2-}$ is quickly depleted under operating condition, we propose that aqueous CO_2 reduction by immobilized **CoPcP** follows a different pathway to that previously suggested for hybrid-**CoPc** electrodes.[30,58,66] In particular, the catalytic mechanism of **CoPcP** proceeds *via* binding of CO_2 to $[\textbf{CoPcP}]^{2-}$ followed by protonation and reduction of the $[\textbf{CoPcP}\bullet CO_2H]^{-}$ adduct. Unlike earlier studies that suggested that the catalytic cycle of **CoPc** involves two e^- transfer steps and a rate-limiting CO_2 binding to $[\textbf{CoPc}]^{-}$ or $[\textbf{CoPc}]^{2-}$, we propose that the third e^- transfer step is the ratedetermining step in our **CoPcP** system because a slow CO_2 binding would have led to build-up of [**CoPcP**]$^{2-}$ under steady state operating condition ($E_{app} \leq -0.89$ V). The proposed mechanism is illustrated in Figure 3d which is similar to that described in a previous report on CO_2 reduction by **CoPc** in organic systems.[64]

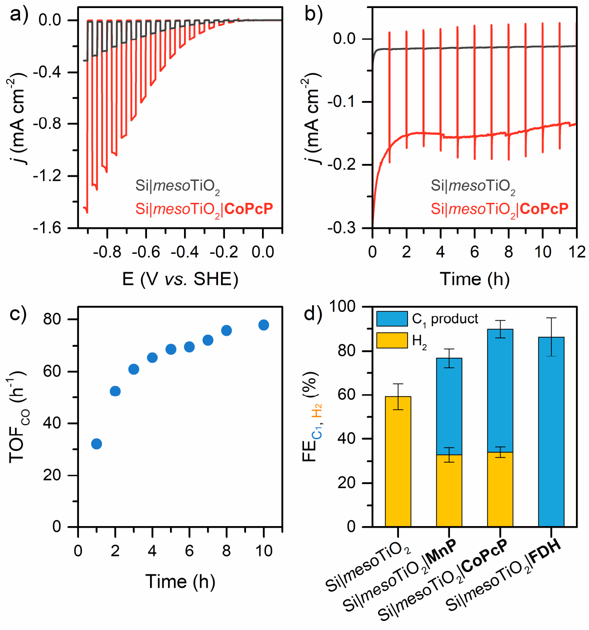

Figure 4. PEC studies of Si|*meso*TiO_2|**CoPcP** and control experiments: (a) LSVs of Si|*meso*TiO_2 and Si|*meso*TiO_2|**CoPcP** under CO_2 with chopped illumination at 5 mV s^{-1} scan rate; (b) CPPE traces at $E_{app} = -0.53$ V *vs.* SHE with Si|*meso*TiO_2 and Si|*meso*TiO_2|**CoPcP** photocathodes under continuous illumination and an hourly one min dark chop; (c) variation of TOF_{CO} (cumulative) during CPPE; (d) Faradaic efficiencies for C_1-product (CO and HCOOH, denoted as FE_{C1}) and H_2 (FE_{H_2}) generated by Si|*meso*TiO_2|**CoPcP**, Si|*meso*TiO_2|**MnP** and Si|*meso*TiO_2|**FDH** after 12 h CPPE at $E_{app} = -0.53$ V *vs.* SHE. A tabulated summary of CPPE results is provided in Supporting Information, Table S5. Conditions: 0.5 M $KHCO_3$, 100 mW cm^{-2}, AM 1.5G, λ > 400 nm, room temperature.

Having established high performance and stability of *meso*TiO_2|**CoPcP** for electrocatalytic CO_2 reduction in the absence of external illumination, we aimed to utilize this molecule-material hybrid assembly in solar-driven CO_2 conversion by integrating it with a *p*-type Si photoelectrode. The Si|*meso*TiO_2|**CoPcP** photocathode was assembled by first depositing the stabilizing mesoporous TiO_2 scaffold on freshly etched planar Si,[67] followed by immobilization of **CoPcP** by soaking in DMSO/MeOH solution ($^{\text{UV-vis}}\Gamma_{\mathbf{CoPcP}} = 22.4 \pm 1.6$ nmol cm^{-2}). The photocathode was washed with

DMSO and MeOH, and dried in air prior to use. LSVs with chopped illumination in CO_2-saturated electrolyte (0.5 M $KHCO_3$, pH 7.3) revealed a comparable photocurrent onset potential (E_{onset}) at –0.15 and –0.19 V *vs.* SHE for Si|*meso*TiO_2|**CoPcP** and bare Si|*meso*TiO_2 electrode, respectively, but a higher photocurrent response in the presence of **CoPcP** (Figure 4a). This result agrees with previous studies that the Si|*meso*TiO_2 photoelectrodes act like a buried junction, controlled by the p–n Si–*meso*TiO_2 interface, and deliver a photovoltage of 550–600 mV.[67-69]

Controlled potential photoelectrolysis (CPPE) in aqueous electrolyte solution (0.5 M $KHCO_3$, pH 7.3) confirmed photoreduction of CO_2 by photoexcited Si to **CoPcP** *via* the conduction band of the mesoporous TiO_2 interlayer. CPPE with a Si|*meso*TiO_2|**CoPcP** electrode maintained at E_{app} = –0.53 V *vs.* SHE with front illumination (AM1.5G, 100 mW cm^{-2}, λ > 400 nm to avoid TiO_2 band gap excitation) produced 21 ± 3 μmol CO cm^{-2} and 11 ± 1.6 μmol H_2 cm^{-2} over the course of 12 h with a total FE of (85 ± 2)% (FE_{CO} = (56 ± 4)%) and a total TON_{CO+H_2} of 1430 ± 150 (TON_{CO} = 939 ± 132). A stable photocurrent of approximately –150 μA cm^{-2} was observed with CO selectivity at (66 ± 3)% (CO:H_2 = 1.9 ± 0.3) (Figure 4b). Continuous monitoring of the headspace gas shows an initial (0–4 h) increase of turnover frequency for CO production (TOF_{CO}, h^{-1}) which plateaus to a steady rate of ~70 h^{-1}, implying a stable photocathode assembly (Figure 4c). The early increase could be attributed to the reduction of O_2 trapped in *meso*TiO_2 and slow release of CO and H_2 from the mesoporous scaffold which is supported by the observed increase in total FE over time (Figure S22). Post-CPPE UV-vis spectroscopy of desorbed **CoPcP** confirms that the molecular structure of **CoPcP** remains intact but shows a loss of ~20% immobilized catalyst over 12 h (Figure S12b and Table S3). Nonetheless, the photocathode assembly maintains a constant activity over several hours operating at near thermodynamic potential for CO_2-to-CO conversion ($E^{0'}_{CO_2/CO}$ = –0.54 V *vs.* SHE).

To demonstrate the versatility of the Si|*meso*TiO_2 platform and evaluate the PEC activity of **CoPcP**, CPPE was conducted with two analogous PEC systems that featured the synthetic molecular catalyst **MnP**,[40] and the enzyme, **FDH**, immobilized on Si|*meso*TiO_2 (Table S5). A long pass cut-off filter (λ > 590 nm) was employed for CPPE of Si|*meso*TiO_2|**MnP** to circumvent the photosensitivity of the catalyst, whereas a standard UV-cut-off filter (λ > 400 nm) was used for Si|*meso*TiO_2|**FDH**. **CoPcP**

(TON_{CO} = 939 after 12 h) compared favorably to **MnP** (TON_{CO} = 342 after 12 h), with both showing a similar CO selectivity (60–66%) and **MnP** displaying a steady decrease in photocurrent over time (Figure S23). However, it is worth noting that despite the lower energy and intensity of the filtered light (λ > 590 nm), **MnP** performs efficiently with high TON_{CO} and CO-selectivity. **FDH** has been demonstrated previously to anchor strongly on metal-oxide surfaces (ITO and TiO_2), and the hybrid **FDH**-bioelectrodes to catalyze the electrochemical reduction of CO_2 to formate with high efficiency through fast, direct interfacial electron transfer.[54,70] **FDH** (160 pmol) was drop-coated on Si|*meso*TiO_2 under inert atmosphere to construct Si|*meso*TiO_2|**FDH**, which displays a stable photocurrent of approximately –70 μA cm^{-2}, yielding formate as the sole product (FE = 99%) and a TON_{HCOO^-} of ~14500 (Figure S23 and Table S5). Although the **FDH**-photocathode exhibits the highest selectivity towards CO_2 reduction among the three catalysts, the large footprint of **FDH** limits the amount of enzyme that can be loaded on the Si|*meso*TiO_2 scaffold, resulting in a lower photocurrent compared to **CoPcP** and **MnP**. This highlights the need for macromolecule-accommodating mesoporous and macroporous substrates for the development of bio-hybrid systems.[68,71]

Previously reported molecular photocathodes for aqueous CO_2 reduction commonly employed noble-metal-based co-catalysts,[11,13-15,21,22] whereas precious-metal-free photocathodes required organic solvents or mixed organic-aqueous medium to achieve selective CO_2 reduction.[18,19,25] The Si|*meso*TiO_2|**CoPcP** electrode catalyzes PEC CO_2-to-CO reduction in purely aqueous solution with 56% FE_{CO}, displaying a photocurrent of –150 μA cm^{-2} and achieving a TON_{CO} as high as 939 after 12 h. This outperforms almost all of the previously studied molecular photocathodes including both earth-abundant and noble-metal-based systems (Table S6), and is only out-performed by the recently reported benchmark Co-quaterpyridine/CIGS photocathode (CIGS|f-TiO_2|**Co-qPyH**) that displays a photocurrent of –800 μA cm^{-2}, a TON_{CO} of 8031, and a FE_{CO} of 87% after 2 h.[24] Interestingly, the catalyst metrics (current density, TON and selectivity) displayed by Si|*meso*TiO_2|**CoPcP** photoelectrode during CPPE at −0.53 V *vs.* SHE are matched by Ti|*meso*TiO_2|**CoPcP** electrode when CPE is conducted at −0.89 V *vs*. SHE (Figure S24, Table S2 and S5). The slightly lower CO evolution rate displayed by Si|*meso*TiO_2|**CoPcP** could be due to the intense absorption of the immobilized **CoPcP** in the visible region which lowers the amount of light reaching Si.

Conclusions

In summary, we introduce **CoPcP** as a versatile phthalocyanine-based molecular CO_2-reduction catalyst that allows for robust immobilization on metal-oxide surfaces with its four phosphonic acid anchoring groups. The assembled *meso*TiO_2|**CoPcP** cathode achieved efficient CO_2 reduction to CO with 85% selectivity, reaching a high TON_{CO} of 1949 ± 5 after 2 h CPE at –1.09 V *vs.* SHE. Transparency of TiO_2 and its conductivity at reducing potentials enabled mechanistic investigations of *meso*TiO_2|**CoPcP** hybrid by in situ spectroelectrochemistry. Lack of build-up of the doubly reduced species, [**CoPcP**]$^{2-}$, under steady state electrocatalysis condition indicated that, rather than CO_2 binding, a third e^- transfer step involving reduction of [**CoPcP**]$^{2-}$•CO_2 adduct is rate limiting. To integrate this assembly into a solar-driven PEC system, a Si|*meso*TiO_2|**CoPcP** photocathode was fabricated that delivers good performance towards PEC CO_2 reduction in water, demonstrating the ability of **CoPcP** to harvest the conduction band electrons from $TiO_2$for catalysis. Furthermore, catalytic activity of **CoPcP** was evaluated against another small molecule catalyst (**MnP**), a polymeric catalyst (**CoPolyPc**), and an enzyme (**FDH**) under electrochemical and PEC conditions, which shows that **CoPcP** compare favorably to other synthetic catalysts with respect to TONs and selectivity. While FDH delivers much superior selectivity towards C1 product and high TONs, **CoPcP** offers other advantages including easier handling, better scalability and durability while maintaining good selectivity towards CO. Interestingly, **CoPcP** delivers better performance than the recently reported Co-quaterpyridine catalyst (**CoqPyH**) in electrolysis experiments, but when PEC CO_2 reduction is considered, Si|*meso*TiO_2|**CoPcP** displays a lower activity than a CIGS|f-TiO_2|**Co-qPyH** photocathode.[24] This suggests scope for further improvement of our system by combining **CoPcP** with other light absorbing materials. However, it should be noted that Si has the added benefits of low cost and scalability compared to CIGS, which is not yet technologically and commercially ready for large-scale deployment. Overall, this work presents a rare example of a precious-metal-free metal-oxide based hybrid (photo)electrode for aqueous CO_2 reduction, and paves the way for future development of tandem PEC devices featuring CO_2-reducing photocathodes paired with suitable photoanodes.

Supporting Information. Synthetic details for **CoPcP**, ^{1}H and ^{13}C NMR of the compounds, SEM images of *meso*TiO2|**CoPcP** electrodes with EDX mapping, XPS data, additional data on electrolysis, photoelectrolysis and gas chromatography, $^{13}CO_2$ labelling experiment and spectroelectrochemical data on *meso*ITO electrodes.

Acknowledgements. This work was supported by the European Commission's Horizon 2020 research and innovation program with a Marie Skłodowska-Curie Fellowship (CO2RED, GAN745604; S. R.) and an ERC Consolidator Grant (MatEnSAP; 682833; M. M. and E. R.), the Christian Doppler Research Association (Austrian Federal Ministry for Digital and Economic Affairs, the National Foundation for Research, Technology and Development) and the OMV Group (J. W., C. D. S., and E. R.), and the Woolf Fisher Trust in New Zealand (J. J. L.). The authors thank Mr. Adam Brown for XPS measurements, Dr. Carla Casadevall for help with Native MS, and Prof Inês A. C. Pereira and Ms. Ana Rita Oliveira for a sample of FDH.

References

(1) Spitler, M. T.; Modestino, M. A.; Deutsch, T. G.; Xiang, C. X.; Durrant, J. R.; Esposito, D. V.; Haussener, S.; Maldonado, S.; Sharp, I. D.; Parkinson, B. A.; Ginley, D. S.; Houle, F. A.; Hannappel, T.; Neale, N. R.; Nocera, D. G.; McIntyre, P. C. Practical challenges in the development of photoelectrochemical solar fuels production. *Sustainable Energy Fuels* **2020**, *4*, 985-995.

(2) Zhang, L.; Zhao, Z.-J.; Wang, T.; Gong, J. Nano-designed semiconductors for electro- and photoelectro-catalytic conversion of carbon dioxide. *Chem. Soc. Rev.* **2018**, *47*, 5423-5443.

(3) Dalle, K. E.; Warnan, J.; Leung, J. J.; Reuillard, B.; Karmel, I. S.; Reisner, E. Electro- and Solar-Driven Fuel Synthesis with First Row Transition Metal Complexes. *Chem. Rev.* **2019**, *119*, 2752-2875.

(4) Zhao, J.; Wang, X.; Xu, Z.; Loo, J. S. C. Hybrid catalysts for photoelectrochemical reduction of carbon dioxide: a prospective review on semiconductor/metal complex co-catalyst systems. *J. Mater. Chem. A* **2014**, *2*, 15228-15233.

(5) Smith, P. T.; Nichols, E. M.; Cao, Z.; Chang, C. J. Hybrid Catalysts for Artificial Photosynthesis: Merging Approaches from Molecular, Materials, and Biological Catalysis. *Acc. Chem. Res.* **2020**, *53*, 575-587.

(6) Torbensen, K.; Joulié, D.; Ren, S.; Wang, M.; Salvatore, D.; Berlinguette, C. P.; Robert, M. Molecular Catalysts Boost the Rate of Electrolytic CO2 Reduction. *ACS Energy Lett.* **2020**, *5*, 1512-1518.

(7) Takeda, H.; Cometto, C.; Ishitani, O.; Robert, M. Electrons, Photons, Protons and Earth-Abundant Metal Complexes for Molecular Catalysis of CO2 Reduction. *ACS Catal.* **2017**, *7*, 70-88.

(8) Cao, Z.; Zacate, S. B.; Sun, X.; Liu, J.; Hale, E. M.; Carson, W. P.; Tyndall, S. B.; Xu, J.; Liu, X.; Liu, X.; Song, C.; Luo, J.-h.; Cheng, M.-J.; Wen, X.; Liu, W. Tuning Gold Nanoparticles with Chelating Ligands for Highly Efficient Electrocatalytic CO2 Reduction. *Angew. Chem. Int. Ed.* **2018**, *57*, 12675-12679.

(9) Gong, M.; Cao, Z.; Liu, W.; Nichols, E. M.; Smith, P. T.; Derrick, J. S.; Liu, Y.-S.; Liu, J.; Wen, X.; Chang, C. J. Supramolecular Porphyrin Cages Assembled at Molecular–Materials Interfaces for Electrocatalytic CO Reduction. *ACS Central Science* **2017**, *3*, 1032-1040.

(10) Kumar, B.; Smieja, J. M.; Kubiak, C. P. Photoreduction of CO2 on p-type Silicon Using Re(bipy-But)(CO)3Cl: Photovoltages Exceeding 600 mV for the Selective Reduction of CO2 to CO. *J. Phys. Chem. C* **2010**, *114*, 14220-14223.

(11) Arai, T.; Sato, S.; Uemura, K.; Morikawa, T.; Kajino, T.; Motohiro, T. Photoelectrochemical reduction of CO2 in water under visible-light irradiation by a p-type InP photocathode modified with an electropolymerized ruthenium complex. *Chem. Commun.* **2010**, *46*, 6944-6946.

(12) Sato, S.; Arai, T.; Morikawa, T.; Uemura, K.; Suzuki, T. M.; Tanaka, H.; Kajino, T. Selective CO2 Conversion to Formate Conjugated with H2O Oxidation Utilizing Semiconductor/Complex Hybrid Photocatalysts. *J. Am. Chem. Soc.* **2011**, *133*, 15240-15243.

(13) Arai, T.; Sato, S.; Kajino, T.; Morikawa, T. Solar CO2 reduction using H2O by a semiconductor/metal-complex hybrid photocatalyst: enhanced efficiency and demonstration of a wireless system using SrTiO3 photoanodes. *Energy Environ. Sci.* **2013**, *6*, 1274-1282.

(14) Sahara, G.; Kumagai, H.; Maeda, K.; Kaeffer, N.; Artero, V.; Higashi, M.; Abe, R.; Ishitani, O. Photoelectrochemical Reduction of CO2 Coupled to Water Oxidation Using a Photocathode with a Ru(II)–Re(I) Complex Photocatalyst and a CoOx/TaON Photoanode. *J. Am. Chem. Soc.* **2016**, *138*, 14152-14158.

(15) Li, T.-T.; Shan, B.; Meyer, T. J. Stable Molecular Photocathode for Solar-Driven CO2 Reduction in Aqueous Solutions. *ACS Energy Lett.* **2019**, *4*, 629-636.

(16) Beley, M.; Collin, J.-P.; Sauvage, J.-P.; Petit, J.-P.; Chartier, P. Photoassisted electro-reduction of CO2 on p-GaAs in the presence of Ni cyclam2+. *Journal of Electroanalytical Chemistry and Interfacial Electrochemistry* **1986**, *206*, 333-339.

(17) Bradley, M. G.; Tysak, T.; Graves, D. J.; Viachiopoulos, N. A. Electrocatalytic reduction of carbon dioxide at illuminated p-type silicon semiconduccting electrodes. *J. Chem. Soc., Chem. Commun.* **1983**, 349-350.

(18) He, D.; Jin, T.; Li, W.; Pantovich, S.; Wang, D.; Li, G. Photoelectrochemical CO2 Reduction by a Molecular Cobalt(II) Catalyst on Planar and Nanostructured Si Surfaces. *Chem. Eur. J.* **2016**, *22*, 13064-13067.

(19) Torralba-Peñalver, E.; Luo, Y.; Compain, J.-D.; Chardon-Noblat, S.; Fabre, B. Selective Catalytic Electroreduction of CO2 at Silicon Nanowires (SiNWs) Photocathodes Using Non-Noble Metal-Based Manganese Carbonyl Bipyridyl Molecular Catalysts in Solution and Grafted onto SiNWs. *ACS Catal.* **2015**, *5*, 6138-6147.

(20) Schreier, M.; Gao, P.; Mayer, M. T.; Luo, J.; Moehl, T.; Nazeeruddin, M. K.; Tilley, S. D.; Grätzel, M. Efficient and selective carbon dioxide reduction on low cost protected Cu2O photocathodes using a molecular catalyst. *Energy Environ. Sci.* **2015**, *8*, 855-861.

(21) Schreier, M.; Luo, J.; Gao, P.; Moehl, T.; Mayer, M. T.; Grätzel, M. Covalent Immobilization of a Molecular Catalyst on Cu2O Photocathodes for CO2 Reduction. *J. Am. Chem. Soc.* **2016**, *138*, 1938-1946.

(22) Sekizawa, K.; Sato, S.; Arai, T.; Morikawa, T. Solar-Driven Photocatalytic CO2 Reduction in Water Utilizing a Ruthenium Complex Catalyst on p-Type Fe2O3 with a Multiheterojunction. *ACS Catal.* **2018**, *8*, 1405-1416.

(23) Shan, B.; Vanka, S.; Li, T.-T.; Troian-Gautier, L.; Brennaman, M. K.; Mi, Z.; Meyer, T. J. Binary molecular-semiconductor p–n junctions for photoelectrocatalytic CO2 reduction. *Nat. Energy* **2019**, *4*, 290-299.

(24) Pati, P. B.; Wang, R.; Boutin, E.; Diring, S.; Jobic, S.; Barreau, N.; Odobel, F.; Robert, M. Photocathode functionalized with a molecular cobalt catalyst for selective carbon dioxide reduction in water. *Nat. Commun.* **2020**, *11*, 3499.

(25) Leung, J. J.; Warnan, J.; Ly, K. H.; Heidary, N.; Nam, D. H.; Kuehnel, M. F.; Reisner, E. Solar-driven reduction of aqueous CO2 with a cobalt bis(terpyridine)-based photocathode. *Nat. Catal.* **2019**, *2*, 354-365.

(26) Lieber, C. M.; Lewis, N. S. Catalytic reduction of carbon dioxide at carbon electrodes modified with cobalt phthalocyanine. *J. Am. Chem. Soc.* **1984**, *106*, 5033-5034.

(27) Meshitsuka, S.; Ichikawa, M.; Tamaru, K. Electrocatalysis by metal phthalocyanines in the reduction of carbon dioxide. *J. Chem. Soc., Chem. Commun.* **1974**, 158-159.

(28) Kapusta, S.; Hackerman, N. Carbon Dioxide Reduction at a Metal Phthalocyanine Catalyzed Carbon Electrode. *J. Electrochem. Soc.* **1984**, *131*, 1511-1514.

(29) Wang, M.; Torbensen, K.; Salvatore, D.; Ren, S.; Joulié, D.; Dumoulin, F.; Mendoza, D.; Lassalle-Kaiser, B.; Işci, U.; Berlinguette, C. P.; Robert, M. CO2 electrochemical catalytic reduction with a highly active cobalt phthalocyanine. *Nat. Commun.* **2019**, *10*, 3602.

(30) Liu, Y.; McCrory, C. C. L. Modulating the mechanism of electrocatalytic CO2 reduction by cobalt phthalocyanine through polymer coordination and encapsulation. *Nat. Commun.* **2019**, *10*, 1683.

(31) Ren, S.; Joulié, D.; Salvatore, D.; Torbensen, K.; Wang, M.; Robert, M.; Berlinguette, C. P. Molecular electrocatalysts can mediate fast, selective CO<sub>2</sub> reduction in a flow cell. *Science* **2019**, *365*, 367.

(32) Han, N.; Wang, Y.; Ma, L.; Wen, J.; Li, J.; Zheng, H.; Nie, K.; Wang, X.; Zhao, F.; Li, Y.; Fan, J.; Zhong, J.; Wu, T.; Miller, D. J.; Lu, J.; Lee, S.-T.; Li, Y. Supported Cobalt Polyphthalocyanine for High-Performance Electrocatalytic CO2 Reduction. *Chem* **2017**, *3*, 652-664.

(33) Yang, Z.; Zhang, X.; Long, C.; Yan, S.; Shi, Y.; Han, J.; Zhang, J.; An, P.; Chang, L.; Tang, Z. Covalently anchoring cobalt phthalocyanine on zeolitic imidazolate frameworks for efficient carbon dioxide electroreduction. *CrystEngComm* **2020**, *22*, 1619-1624.

(34) Huai, M.; Yin, Z.; Wei, F.; Wang, G.; Xiao, L.; Lu, J.; Zhuang, L. Electrochemical CO2 reduction on heterogeneous cobalt phthalocyanine catalysts with different carbon supports. *Chem. Phys. Lett.* **2020**, *754*, 137655.

(35) Huang, N.; Lee, K. H.; Yue, Y.; Xu, X.; Irle, S.; Jiang, Q.; Jiang, D. A Stable and Conductive Metallophthalocyanine Framework for Electrocatalytic Carbon Dioxide Reduction in Water. *Angew. Chem. Int. Ed.* **2020**, *59*, 16587-16593.

(36) Roy, S.; Reisner, E. Visible-Light-Driven CO2 Reduction by Mesoporous Carbon Nitride Modified with Polymeric Cobalt Phthalocyanine. *Angew. Chem. Int. Ed.* **2019**, *58*, 12180-12184.

(37) Rosser, T. E.; Reisner, E. Understanding Immobilized Molecular Catalysts for Fuel-Forming Reactions through UV/Vis Spectroelectrochemistry. *ACS Catal.* **2017**, *7*, 3131-3141.

(38) Mersch, D.; Lee, C.-Y.; Zhang, J. Z.; Brinkert, K.; Fontecilla-Camps, J. C.; Rutherford, A. W.; Reisner, E. Wiring of Photosystem II to Hydrogenase for Photoelectrochemical Water Splitting. *J. Am. Chem. Soc.* **2015**, *137*, 8541-8549.

(39) Muresan, N. M.; Willkomm, J.; Mersch, D.; Vaynzof, Y.; Reisner, E. Immobilization of a Molecular Cobaloxime Catalyst for Hydrogen Evolution on a Mesoporous Metal Oxide Electrode. *Angew. Chem. Int. Ed.* **2012**, *51*, 12749-12753.

(40) Rosser, T. E.; Windle, C. D.; Reisner, E. Electrocatalytic and Solar-Driven CO2 Reduction to CO with a Molecular Manganese Catalyst Immobilized on Mesoporous TiO2. *Angew. Chem. Int. Ed.* **2016**, *55*, 7388-7392.

(41) Mohamed, E. A.; Zahran, Z. N.; Naruta, Y. Efficient Heterogeneous CO2 to CO Conversion with a Phosphonic Acid Fabricated Cofacial Iron Porphyrin Dimer. *Chem. Mater.* **2017**, *29*, 7140-7150.

(42) Wang, Y.; Marquard, S. L.; Wang, D.; Dares, C.; Meyer, T. J. Single-Site, Heterogeneous Electrocatalytic Reduction of CO2 in Water as the Solvent. *ACS Energy Lett.* **2017**, *2*, 1395-1399.

(43) Materna, K. L.; Crabtree, R. H.; Brudvig, G. W. Anchoring groups for photocatalytic water oxidation on metal oxide surfaces. *Chem. Soc. Rev.* **2017**, *46*, 6099-6110.

(44) Görlach, B.; Dachtler, M.; Glaser, T.; Albert, K.; Hanack, M. Synthesis and Separation of Structural Isomers of 2(3),9(10),16(17),23(24)-Tetrasubstituted Phthalocyanines. *Chem. Eur. J.* **2001**, *7*, 2459-2465.

(45) Liao, M.-S.; Scheiner, S. Electronic structure and bonding in metal phthalocyanines, Metal=Fe, Co, Ni, Cu, Zn, Mg. *J. Chem. Phys.* **2001**, *114*, 9780-9791.

(46) Wadsworth, B. L.; Beiler, A. M.; Khusnutdinova, D.; Jacob, S. I.; Moore, G. F. Electrocatalytic and Optical Properties of Cobaloxime Catalysts Immobilized at a Surface-Grafted Polymer Interface. *ACS Catal.* **2016**, *6*, 8048-8057.

(47) Willkomm, J.; Muresan, N. M.; Reisner, E. Enhancing H2 evolution performance of an immobilised cobalt catalyst by rational ligand design. *Chem. Sci.* **2015**, *6*, 2727-2736.

(48) Leung, J. J.; Vigil, J. A.; Warnan, J.; Edwardes Moore, E.; Reisner, E. Rational Design of Polymers for Selective CO2 Reduction Catalysis. *Angew. Chem. Int. Ed.* **2019**, *58*, 7697-7701.

(49) Vinodgopal, K.; Bedja, I.; Kamat, P. V. Nanostructured Semiconductor Films for Photocatalysis. Photoelectrochemical Behavior of SnO2/TiO2 Composite Systems and Its Role in Photocatalytic Degradation of a Textile Azo Dye. *Chem. Mater.* **1996**, *8*, 2180-2187.

(50) Tasso, T. T.; Furuyama, T.; Kobayashi, N. Absorption and Electrochemical Properties of Cobalt and Iron Phthalocyanines and Their Quaternized Derivatives: Aggregation Equilibrium and Oxygen Reduction Electrocatalysis. *Inorg. Chem.* **2013**, *52*, 9206-9215.

(51) Bard, A. J.; Parsons, R.; Jordan, J.: *Standard potentials in aqueous solution*; Marcel Dekker, Inc.,New York, NY: United States, 1985.

(52) Oliveira, A. R.; Mota, C.; Mourato, C.; Domingos, R. M.; Santos, M. F. A.; Gesto, D.; Guigliarelli, B.; Santos-Silva, T.; Romão, M. J.; Cardoso Pereira, I. A. Toward the Mechanistic Understanding of Enzymatic CO2 Reduction. *ACS Catal.* **2020**, *10*, 3844-3856.

(53) da Silva, S. M.; Voordouw, J.; Leitão, C.; Martins, M.; Voordouw, G.; Pereira, I. A. C. Function of formate dehydrogenases in Desulfovibrio vulgaris Hildenborough energy metabolism. *Microbiology* **2013**, *159*, 1760-1769.

(54) Miller, M.; Robinson, W. E.; Oliveira, A. R.; Heidary, N.; Kornienko, N.; Warnan, J.; Pereira, I. A. C.; Reisner, E. Interfacing Formate Dehydrogenase with Metal Oxides for the Reversible Electrocatalysis and Solar-Driven Reduction of Carbon Dioxide. *Angew. Chem. Int. Ed.* **2019**, *58*, 4601-4605.

(55) Hod, I.; Sampson, M. D.; Deria, P.; Kubiak, C. P.; Farha, O. K.; Hupp, J. T. Fe-Porphyrin-Based Metal–Organic Framework Films as High-Surface Concentration, Heterogeneous Catalysts for Electrochemical Reduction of CO2. *ACS Catal.* **2015**, *5*, 6302-6309.

(56) Fang, Y.-H.; Liu, Z.-P. Tafel Kinetics of Electrocatalytic Reactions: From Experiment to First-Principles. *ACS Catal.* **2014**, *4*, 4364-4376.

(57) Morlanés, N.; Takanabe, K.; Rodionov, V. Simultaneous Reduction of CO2 and Splitting of H2O by a Single Immobilized Cobalt Phthalocyanine Electrocatalyst. *ACS Catal.* **2016**, *6*, 3092-3095.

(58) Zhu, M.; Ye, R.; Jin, K.; Lazouski, N.; Manthiram, K. Elucidating the Reactivity and Mechanism of CO2 Electroreduction at Highly Dispersed Cobalt Phthalocyanine. *ACS Energy Lett.* **2018**, *3*, 1381-1386.

(59) Zhu, M.; Chen, J.; Guo, R.; Xu, J.; Fang, X.; Han, Y.-F. Cobalt phthalocyanine coordinated to pyridine-functionalized carbon nanotubes with enhanced CO2 electroreduction. *Appl. Catal., B* **2019**, *251*, 112-118.

(60) Manbeck, G. F.; Fujita, E. A review of iron and cobalt porphyrins, phthalocyanines and related complexes for electrochemical and photochemical reduction of carbon dioxide. *J. Porphyrins Phthalocyanines* **2015**, *19*, 45-64.

(61) Nevin, W. A.; Liu, W.; Greenberg, S.; Hempstead, M. R.; Marcuccio, S. M.; Melnik, M.; Leznoff, C. C.; Lever, A. B. P. Synthesis, aggregation, electrocatalytic activity, and redox properties of a tetranuclear cobalt phthalocyanine. *Inorg. Chem.* **1987**, *26*, 891-899.

(62) Nevin, W. A.; Hempstead, M. R.; Liu, W.; Leznoff, C. C.; Lever, A. B. P. Electrochemistry and spectroelectrochemistry of mononuclear and binuclear cobalt phthalocyanines. *Inorg. Chem.* **1987**, *26*, 570-577.

(63) Le Moigne, J.; Even, R. Spectroscopic properties and conductivity of thin films of partially reduced metallo-phthalocyanines. *J. Chem. Phys.* **1985**, *83*, 6472-6479.

(64) Abe, T.; Yoshida, T.; Tokita, S.; Taguchi, F.; Imaya, H.; Kaneko, M. Factors affecting selective electrocatalytic co2 reduction with cobalt phthalocyanine incorporated in a polyvinylpyridine membrane coated on a graphite electrode. *J. Electroanal. Chem.* **1996**, *412*, 125-132.

(65) Abe, T.; Imaya, H.; Yoshida, T.; Tokita, S.; Schlettwein, D.; Wöhrle, D.; Kaneko, M. Electrochemical CO2 Reduction Catalysed by Cobalt Octacyanophthalocyanine and its Mechanism. *J. Porphyrins Phthalocyanines* **1997**, *01*, 315-321.

(66) Choi, J.; Wagner, P.; Gambhir, S.; Jalili, R.; MacFarlane, D. R.; Wallace, G. G.; Officer, D. L. Steric Modification of a Cobalt Phthalocyanine/Graphene Catalyst To Give Enhanced and Stable Electrochemical CO2 Reduction to CO. *ACS Energy Lett.* **2019**, *4*, 666-672.

(67) Leung, J. J.; Warnan, J.; Nam, D. H.; Zhang, J. Z.; Willkomm, J.; Reisner, E. Photoelectrocatalytic H2 evolution in water with molecular catalysts immobilised on p-Si via a stabilising mesoporous TiO2 interlayer. *Chem. Sci.* **2017**, *8*, 5172-5180.

(68) Nam, D. H.; Zhang, J. Z.; Andrei, V.; Kornienko, N.; Heidary, N.; Wagner, A.; Nakanishi, K.; Sokol, K. P.; Slater, B.; Zebger, I.; Hofmann, S.; Fontecilla-Camps, J. C.; Park, C. B.; Reisner, E. Solar Water Splitting with a Hydrogenase Integrated in Photoelectrochemical Tandem Cells. *Angew. Chem. Int. Ed.* **2018**, *57*, 10595-10599.

(69) Seger, B.; Pedersen, T.; Laursen, A. B.; Vesborg, P. C. K.; Hansen, O.; Chorkendorff, I. Using TiO2 as a Conductive Protective Layer for Photocathodic H2 Evolution. *J. Am. Chem. Soc.* **2013**, *135*, 1057-1064.

(70) Sokol, K. P.; Robinson, W. E.; Oliveira, A. R.; Warnan, J.; Nowaczyk, M. M.; Ruff, A.; Pereira, I. A. C.; Reisner, E. Photoreduction of CO2 with a Formate Dehydrogenase Driven by Photosystem II Using a Semi-artificial Z-Scheme Architecture. *J. Am. Chem. Soc.* **2018**, *140*, 16418-16422.

(71) Fang, X.; Kalathil, S.; Reisner, E. Semi-biological approaches to solar-to-chemical conversion. *Chem. Soc. Rev.* **2020**, *49*, 4926-4952.

ToC artwork

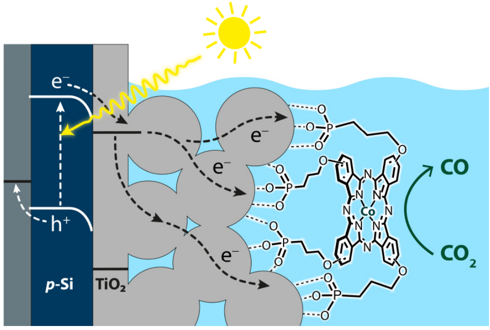

A novel cobalt phthalocyanine catalyst with four phosphonic acid anchors forms a functional CO_2 reduction catalyst upon immobilization on porous metal oxides. The resulting hybrid molecular electrodes enable aqueous CO_2 reduction to CO with high selectivity driven by electricity and, upon integration onto *p*-silicon, by solar energy.